PHYSICAL REVIEW B VOLUME 43, NUMBER 3 15 JANUARY 1991-II

Piezomodulation spectroscopy: A powerful investigation tool of heterostructures

H. Mathieu, J. Allègre, and B. Gil

Groupe d'Etudes des Semiconducteurs, Université des Sciences et Techniques du Lanquedoc, place E. Bataillon, 34095 Montpellier CEDEX, France

(Received 12 April 1990)

We discuss the potential of piezomodulated spectroscopy to identify electron and/or hole states, together with their spatial localizations, in strained epilayers, quantum wells, and superlattices. The potential of the technique is illustrated using several experimental results concerning $GaAs/Ga_xAl_{1-x}As$, CdTe/ZnTe, and $CdTe/Cd_xZn_{1-x}Te$ heterostructures.

I. INTRODUCTION

Up to now, most of the work performed in modulated spectroscopy has dealt with three-dimensional (3D) materials and has used both the high resolution of the technique to obtain accurate measurements of optical structures and the localized origin of the response to identify the corresponding critical points in the Brillouin zone. A clear review is given in Ref. 1. More recently, namely only a few years ago, these techniques were extended to the study of heterostructures such as epilayers, quantum wells, and superlattices.[2-8] In modulated spectroscopy, it is necessary to distinguish between two main categories of modulation techniques: internal and external. External modulation techniques consist of perturbing an incident-light parameter such as the wavelength. This results in so-called "wavelength-modulation spectroscopy" (WMS). Internal modulation techniques need a periodic perturbation applied to the sample; this modifies some physical parameter of the semiconductor. These techniques generally use the optical response of the solid, associated with changes in the electronic states, as a function of (a) electric field [electromodulation spectroscopy (EMS)], (b) strain [piezomodulation spectroscopy (PMS)], (c) heat [thermomodulation spectroscopy (TMS)], or (d) light [photo-modulation spectroscopy (PhMS)].

Concerning PMS, it is worth noting that, depending on the relative magnitude of the stress dependencies of electronic states, different electronic transitions are not modulated in the same way. In WMS, on the other hand, the modulation parameter is the same for all electronic transitions. This is the main difference between PMS and WMS, which, however, give rise to comparable line shapes for the optical structures. In other words, PMS and WMS give rise to similar optical responses, but the first is a selective modulation technique, while the second is a nonselective one. The purpose of the present paper is to bring out the potential of PMS for the identification of electron and/or hole states in quantum wells and superlattices.

II. THEORETICAL BACKGROUND

The optical properties of a solid are fully described by the dielectric function

$$\epsilon(\omega)=\epsilon_1(\omega)+i\epsilon_2(\omega) , \tag{1}$$

which is related to the optical functions $n(\omega)$ and $k(\omega)$ by

$$\epsilon_1(\omega)=n^2(\omega)-k^2(\omega), \quad \epsilon_2(\omega)=2n(\omega)k(\omega) . \tag{2}$$

Real and imaginary parts of the dielectric function are connected by the well-known Kramers-Kronig relations,

$$\epsilon_1(\omega)=1+\frac{1}{\pi}\int_0^\infty \frac{\omega'\epsilon_2(\omega')}{\omega'^2-\omega^2}d\omega' , \tag{3a}$$

$$\epsilon_2(\omega)=\frac{2\omega}{\pi}\int_0^\infty \frac{\epsilon_1(\omega')}{\omega^2-\omega'^2}d\omega . \tag{3b}$$

The main optical techniques used to study semiconductor heterostructures are reflectivity, absorption, photoluminescence, and photoluminescence-excitation spectroscopy.

Reflectivity experiments consist of measuring the reflected intensity $I_r(\omega)$, which is the product of the reflectivity coefficient $R(\omega)$ and the intensity of the incident beam. The signal $I_r(\omega)/I_0(\omega)$ is proportional, at each wavelength, to the reflectivity coefficient $R(\omega)$. At normal incidence, Fresnel's formula gives

$$\begin{aligned}\frac{I_r(\omega)}{I_0(\omega)}&=R(\omega)\\ &=\frac{(n-1)^2+k^2}{(n+1)^2+k^2}\\ &=\frac{(\epsilon_1^2+\epsilon_2^2)\pm[2\epsilon_1+2(\epsilon_1^2+\epsilon_2^2)^{1/2}]^{1/2}+1}{[\epsilon_1^2+2(\epsilon_1^2+\epsilon_2^2)^{1/2}]^{1/2}+1} .\end{aligned} \tag{4}$$

Transmission experiments consist of measurements of the transmitted intensity $I_t(\omega)$, which is the product of the transmission coefficient $T(\omega)$ and the intensity of the incident beam. If the contribution due to multiple internal reflections in the sample is neglected, the transmission coefficient is

$$\frac{I_t(\omega)}{I_0(\omega)}=T(\omega)=[1-R(\omega)]^2e^{-K(\omega)d} , \tag{5}$$

where $K(\omega)$ is the absorption coefficient and d the sample thickness. The absorption coefficient is related to the op-

 ©1991 The American Physical Society

tical and dielectric functions by

$$K(\omega)=\frac{2\omega k}{c}=\frac{\omega}{c}\frac{\epsilon_2\sqrt{2}}{[\epsilon_1+(\epsilon_1^2+\epsilon_2^2)^{1/2}]^{1/2}} . \quad (6)$$

Luminescence experiments consist of measuring the wavelength dependence of the spontaneous emitted radiation $I_e(\omega)$ from a sample excited by photons of energy higher than the band gap. Because the oscillator strengths of the downward and upward transitions for an electronic system are identical, the ratio between emission and absorption related to two distributions of levels is a function of the occupation probability of these levels. Now, provided the scattering rate of carriers within a band, or a series of subbands, is fast compared to the recombination rate between bands, or series of subbands, i.e., if the electrons within the conduction subbands and the holes within the valence subbands rapidly establish a quasiequilibrium among themselves, the occupation of these subbands can be characterized by quasi-Fermi-levels:

$$f_c(E)=1/(1+e^{(E-F_c)/kT}) , \quad (7a)$$

$$f_v(E)=1/(1+e^{(F_v-E)/kT}) , \quad (7b)$$

where F_c and F_v are the quasi-Fermi-levels for the conduction and valence band, respectively. For a system in thermal equilibrium, the quasi-Fermi-levels are equal to each other and become the Fermi level. In an excited system, we have $F_c > F_v$ and we can use the difference $\Delta F = F_c - F_v$ as a measure of the excitation. Then, the relation between the spontaneous emission (downward transitions) and the absorption (upward transitions) is[9]

$$I_e(\omega)=\left[\frac{\hbar\omega}{\pi c \hbar^{1/2}}\right]^{1/2}\frac{K(\omega)}{\exp[(\hbar\omega-\Delta F)/kT]} . \quad (8)$$

For semiconductor lasers, the term ΔF is extremely important, with $\Delta F > \hbar\omega$. On the other hand, in luminescence experiments ΔF is smaller than the band gap and Eq. (8) reduces to

$$I_e(\omega)=\left[\frac{\hbar\omega}{\pi c \hbar^{1/2}}\right]^{1/2} e^{\hbar\omega/kT}K(\omega) . \quad (9)$$

For a given transition, the luminescence intensity is then proportional to the corresponding absorption coefficient weighted by the Boltzmann factor.

Luminescence-excitation spectroscopy consists of measuring the amplitude $I_{\omega_e}(\omega_p)$ for the radiation emitted at ω_e, versus pump-photon energy $\hbar\omega_p$. The photon flux of the excitation radiation throughout the material is

$$\phi(\omega_p,x)=\phi_0(\omega_p)[1-R(\omega_p)]e^{-K(\omega_p)x} , \quad (10)$$

where $\phi_0(\omega_p)$ is the incident flux, and $R(\omega_p)$ and $K(\omega_p)$ the reflectivity and absorption coefficients of the material at the frequency ω_p of the pump radiation.

The generation rate of electron-hole pairs is then

$$g(\omega_p,x)=-\frac{d\phi(\omega_p,x)}{dx} . \quad (11)$$

For steady-state excitation, the recombination of electron-hole pairs occurs at the same rate as the generation, so, neglecting diffusion phenomena, the steady-state excess electron and hole concentration at x is given by $\Delta n(\omega_p,x)=\tau g(\omega_p,x)$, where τ is the total lifetime of the carriers.

The intensity of the radiation at frequency ω_e, emitted at the x point inside the material, is given by

$$I_{\omega_e}(\omega_p,x)=\hbar\omega_e\frac{\Delta n(\omega_p,x)}{\tau_{\omega_e}} , \quad (12)$$

where τ_{ω_e} is the radiative lifetime corresponding to the transition investigated.

Now, on account of the isotropic character of the spontaneous emission, the self-absorption of the light emitted and the total internal reflection at the sample surface, only a fraction of the internally generated light reaches the surface, and only a smaller fraction is transmitted through the surface. The externally emitted intensity is

$$I_{\omega_e}(\omega_p)=A(\omega_e)[1-R(\omega_p)]K(\omega_p) \times\int_0^d e^{-[K(\omega_p)+K(\omega_e)]x}dx , \quad (13)$$

where $A(\omega_e)$ contains all phenomena which are function of ω_e, and d is the sample thickness of the active layer. Equation (13) gives

$$I_{\omega_e}(\omega_p)=A(\omega_e)[1-R(\omega_p)]\frac{K(\omega_p)}{K(\omega_p)+K(\omega_e)} \times(1-e^{-[K(\omega_p)+K(\omega_e)]d}) . \quad (14)$$

The self-absorption is generally smaller than the excitation absorption, so Eq. (14) reduces to

$$I_{\omega_e}(\omega_p)=A(\omega_e)[1-R(\omega_p)](1-e^{-K(\omega_p)d}) . \quad (15)$$

The emitted intensity at ω_e is then proportional to the absorption of the pump radiation at ω_p.

Let us now consider modulation spectroscopy. The effect of a sample modulation parameter on the optical properties appears as a change in the real and imaginary parts of the dielectric function. The phenomenological descriptions of the modulated reflectance, transmission, luminescence, and excitation luminescence are given by the total differential of Eqs. (4), (5), (9), and (15), respectively.

The reflectance modulation is

$$\frac{\Delta R}{R}=\alpha(\epsilon_1,\epsilon_2)\Delta\epsilon_1+\beta(\epsilon_1,\epsilon_2)\Delta\epsilon_2 , \quad (16)$$

where α and β are the so-called Seraphin coefficients.[10] The transmission modulation is

$$\frac{\Delta T}{T}=-\frac{2R}{1-R}\frac{\Delta R}{R}-d\,\Delta K-K\,\Delta d . \quad (17)$$

Of the three terms contributing to $\Delta T/T$, the first is generally relatively small compared to the second, and the third term merely produces a background contribution

proportional to K. As a consequence, the second term is usually the leading term, so that $\Delta T/T$ is proportional to the variation ΔK of the absorption coefficient. This is given by the differential of Eq. (6):

$$\Delta K = a(\epsilon_1,\epsilon_2)\Delta\epsilon_1 + b(\epsilon_1,\epsilon_2)\Delta\epsilon_2 \;, \tag{18}$$

where

$$a = -\frac{\pi\sqrt{2}}{\lambda}\frac{\epsilon_2(1+\epsilon_1/A)}{B^3} \;, \tag{19a}$$

$$b = \frac{\pi\sqrt{2}}{\lambda}\frac{2B^2-\epsilon_2^2/A}{B^3} \;, \tag{19b}$$

and $A = (\epsilon_1^2+\epsilon_2^2)^{1/2}$ and $B = (\epsilon_1 + A)^{1/2}$.

In this case the transmission modulation can be written

$$\frac{\Delta T}{T} = da(\epsilon_1,\epsilon_2)\Delta\epsilon_1 + db(\epsilon_1,\epsilon_2)\Delta\epsilon_2 \;. \tag{20}$$

Neglecting the structureless background contribution, the total differential of Eq. (9) gives the modulated luminescence signal:

$$\frac{\Delta I_e}{I_e} = \frac{\Delta K}{K} \;. \tag{21}$$

The spectral structures observed in the experiment are then directly related to the change ΔK for the corresponding absorption coefficient.

Concerning the excitation spectroscopy, it is worth noting that, depending on the technique, the modulation may change both ω_p and ω_e. Now, the aim of the differential excitation spectroscopy is to modulate the exciting radiation, and not the emitted radiation. In this experiment, the emitted radiation acts essentially as a transducer, revealing higher-energy resonances. Then, the resolution of the experimental setup selecting the emitted radiation ω_e must be larger than the linewidth $\Delta\omega_e$ of this radiation. In this case the apparatus integrates a possible modulation of the emitted radiation, and the coefficient $A(\omega_e)$ may be taken as a constant in the derivation of Eq. (15). Then, neglecting the ΔR and Δd contributions as in modulated transmission, the total differential of Eq. (15) gives

$$\frac{\Delta I_e(\omega_p)}{I_e(\omega_p)} = \frac{d}{e^{K(\omega_p)d}-1}\Delta K(\omega_p) \;. \tag{22}$$

In short, the spectral structures observed in modulated reflectivity measurements are related to $\Delta R/R$, and the spectral structures observed in modulated transmission, luminescence, and excitation spectroscopy are essentially related to ΔK. Now, the shapes of $\Delta R/R$ and ΔK, associated with a given transition, are functions, through Eqs. (16) and (18), of the modulations $\Delta\epsilon_1$ and $\Delta\epsilon_2$ of the real and imaginary parts of the dielectric function. The coefficients α,a and β,b weight, respectively, the contribution of $\Delta\epsilon_1$ and $\Delta\epsilon_2$, so the shape of $\Delta R/R$ or ΔK depends on the relative magnitudes of α and β or of a and b. As an example, the values of these coefficients, calculated from values for ϵ_1 and ϵ_2 given by Aspnes *et al.*,[11] are plotted for GaAs in Fig. 1. In particular, at the energy

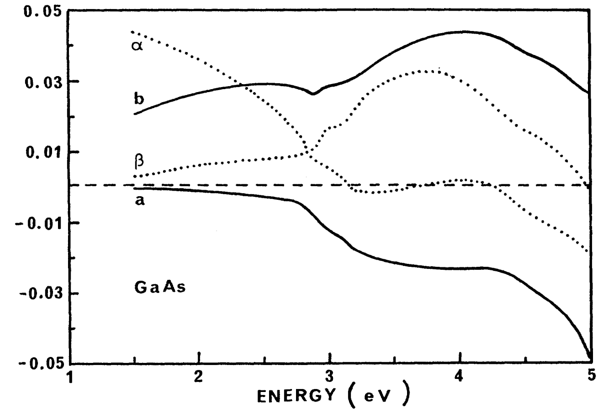

FIG. 1. Fractional coefficients a, b, α, and β in Eqs. (5a) and (5b) for GaAs, from values of ϵ_1 and ϵ_2 given by Aspnes (Ref. 9). α and β are dimensionless; a and b are in units of $(10^2\,\mu\text{m}^{-1})$.

gap $E=1.5$ eV: $\alpha=4.4\times10^{-2}$, $\beta=3\times10^{-3}$, $a=-4.5\times10^{-2}\,\mu\text{m}^{-1}$, and $b=2.1\,\mu\text{m}^{-1}$. These values, which are typical for most semiconductors, clearly show that, for $\Delta R/R$, the low-energy region, containing the fundamental absorption edge, is $\Delta\epsilon_1$, dominated by a value of α much larger than β. For ΔK this low-energy region is $\Delta\epsilon_2$ dominated through a value of b much larger than a. In other words, near the band edge of a 3D semiconductor the reflectivity shape results essentially from the variations in the real part of the dielectric function, and the transmission, luminescence, and excitation-luminescence shapes result essentially from the variations in the imaginary part of the dielectric function. This remains true for 2D materials.

In the differential equations (16) and (18), the coefficients a, b, α, and β are common to all the versions of the modulated spectroscopy, but $\Delta\epsilon_1$ and $\Delta\epsilon_2$ are specific of the modulation technique. Modulation of a sample parameter affects ϵ_1 and ϵ_2 through the joint-density-of-states function near the critical point investigated, $J(E_g,\omega)$. Now, for all types of critical point of three-, two-, or one-dimensional structures, the joint density of states is a function of the spectral distance to E_g; in other words, $J(E_g,\omega)=J(\hbar\omega-E_g)$. Hence, a sample modulation that consists of changing the spectral position of E_g, such as the piezomodulation, gives rise to the same line shape as a light modulation that consists of changing the energy $\hbar\omega$ of the radiation, such as the wavelength modulation. Both optical spectra are then basically similar, keeping in mind that the piezomodulation is selective and the wavelength modulation is not. Consequently, WMS spectra are reference spectra used in order to study the relative modulation amplitudes in PMS. In both cases, the line shape related to ΔK corresponds to the first-order derivative of the imaginary part of the dielectric function, and $\Delta R/R$ corresponds to the first-order derivative of the real part of the dielectric function.

Modulation of the spectral distance $(\hbar\omega-E_g)$ affects ϵ_2 through the joint-density-of-states function $J(\hbar\omega-E_g)$ and ϵ_1 through the differential Kramers-Kronig relations:

$$\Delta\epsilon_2(\omega)=\frac{C}{\omega}\frac{dJ}{d(\hbar\omega-E_g)}\Delta(\hbar\omega-E_g)\ , \tag{23}$$

where C contains the oscillator strength and effective-mass parameters,

$$\Delta\epsilon_1(\omega)=\frac{2}{\pi}\int_0^\infty\frac{\omega'\Delta\epsilon_2(\omega')}{\omega^2-\omega'^2}d\omega' = \frac{2C}{\pi}\int_0^\infty\frac{dJ/d(\hbar\omega-E_g)}{\omega'(\omega^2-\omega'^2)}d\omega'\Delta(\hbar\omega-E_g)\ . \tag{24}$$

In WMS the $\hbar\omega$ modulation is obtained by using a slight modulation of the output mirror of the monochromator. In piezomodulation the E_g modulation results in an alternative stress X applied to the sample, and is written $\Delta E_g=(dE_g/dX)X$.

The basic mechanism of the PMS consists of changing the spectral positions of the energy gap E_g of the samples by mounting them on a piezoelectric transducer. The sample is strained with a typical strain $\Delta l/l$ of the order of 10^{-5}. If the sample is glued to the transducer only at its ends, a uniaxial stress is applied; if, instead, the whole sample surface is glued, the transducer produces a uniform strain in the plane of the sample.

Stress (X) and strain (e) are symmetric second-rank tensors related by a fourth-rank compliance tensor (S):

$$e_{ij}=S_{ijkl}X_{kl}\ , \tag{25}$$

where $\mathbf{e}$ and $\mathbf{X}$ each have only six independent elements and $\mathbf{S}$ reduces, in cubic symmetry, to only three independence nonzero elements. In compact notation, in which the six independent elements of $\mathbf{e}$ and $\mathbf{X}$ are treated as a six-dimensional vector and $\mathbf{S}$ as a second-rank tensor, Eq. (25) is written

$$\begin{bmatrix} e_{xx}\\ e_{yy}\\ e_{zz}\\ 2e_{yz}\\ 2e_{zx}\\ 2e_{xy}\end{bmatrix}=\begin{bmatrix} S_{11} & S_{12} & S_{12} & 0 & 0 & 0\\ S_{12} & S_{11} & S_{12} & 0 & 0 & 0\\ S_{12} & S_{12} & S_{11} & 0 & 0 & 0\\ 0 & 0 & 0 & S_{44} & 0 & 0\\ 0 & 0 & 0 & 0 & S_{44} & 0\\ 0 & 0 & 0 & 0 & 0 & S_{44}\end{bmatrix}\begin{bmatrix} X_{xx}\\ X_{yy}\\ X_{zz}\\ X_{yz}\\ X_{zx}\\ X_{xy}\end{bmatrix}. \tag{26}$$

The modulation of the electronic energy states dE/dX is completely expressed in terms of deformation potentials. Let us consider zinc-blende-type semiconductors. In the bulk material the top of the valence band near $k=0$ is, according to its p character, sixfold degenerate. Part of this degeneracy is lifted by spin-orbit interaction giving rise to the well-known Γ_8 quadruplet of the topmost valence band and the Γ_7 doublet of the split-off band. Quantum-well quantification along the [001] or [111] direction splits the Γ_8 multiplet into doubly-degenerate states $m_j=\pm\frac{3}{2}$, corresponding to heavy holes along the quantization axis, and $m_j=\pm\frac{1}{2}$, corresponding to light holes. So that three separate series of levels are available as initial states for the valence-band–to–conduction-band transitions, another kind of degeneracy is removed by the 2D quantification—one that concerns off-center critical points. The various branches of a multivalley critical point (like X or L minima of the conduction band), equivalent in bulk material, have different projections of their k vector in the direction of the 2D quantization axis, so that an interband splitting results. In a [001] 2D structure the L critical points remain degenerate, but the X critical points split into X_z- and X_{xy}-band extrema. Because of the directional effect, PMS will easily permit an identification of these symmetry-split states.

The energy displacement of the Γ_6 conduction-band minimum is linear in strain and may be written

$$\Delta E_{\Gamma_6}=a_c\mathrm{Tr}e\ , \tag{27}$$

where a_c is the hydrostatic deformation potential of the Γ_6 conduction-band minimum and $\mathrm{Tr}e=e_{xx}+e_{yy}+e_{zz}$.

The energy shift and splitting of the X_6 and L_6 conduction-band minima are given, in the notation of Brooks,[12] by

$$\Delta E_{X_6}=E_1\mathrm{Tr}e+E_2\hat{\mathbf{n}}(\mathbf{e}-\tfrac{1}{3}\mathrm{Tr}e\cdot\boldsymbol{l})\hat{\mathbf{n}}\ , \tag{28a}$$

$$\Delta E_{L_6}=E_1'\mathrm{Tr}e+E_2'\hat{\mathbf{n}}(e-\tfrac{1}{3}\mathrm{Tr}e\cdot\boldsymbol{l})\hat{\mathbf{n}}\ , \tag{28b}$$

where $\hat{\mathbf{n}}$ is a unit vector in direction of the band extrema in k space, $\boldsymbol{l}$ is the unit dyadic, and E_1 (E_1') and E_2 (E_2') are the hydrostatic and shear deformation potentials of the X_6 (L_6) conduction-band minima.

For the Γ_8 valence-band maximum, the stress Hamiltonian is[13,14]

$$H_e=-a_v\mathrm{Tr}e-3b[(L_x^2-\tfrac{1}{3}L^2)e_{xx}+\mathrm{c.p.}] -\frac{6d}{\sqrt{3}}[(L_xL_y)e_{xy}+\mathrm{c.p.}]\ , \tag{29}$$

where L is the angular-momentum operator, c.p. denotes cyclic permutation with respect to the indices x, y, and z, a_v is the hydrostatic deformation potential, and b and d are the tetragonal and trigonal shear deformation potentials of the Γ_8 valence-band maximum.

Now, considering quantum wells and superlattices, it is worth noting that the symmetry axis of the structure, and then the quantization axis, corresponds to the growth direction. So, one should distinguish between in-plane uniaxial-stress modulation and coplanar-stress modulation. In the latter case the heterostructure quantization axis corresponds to the symmetry axis of the stress, and the quantum states of the heterostructure remain eigenstates under stress. PMS only changes the energy values without any level mixing. This is no longer true for an in-plane uniaxial-stress modulation. However, owing to the small magnitude of the energy shift under modulating stress, and unless the energy states are very close to one another, the state mixing may be ignored and all effects of stress may be assumed to be linear.

Generally the growth direction of heterostructures is the [001] axis, so the experimental configuration corresponds to a [001]-symmetry coplanar stress or a [100] uniaxial stress.

Under a [001]-symmetry coplanar stress, the strain-

tensor components are

$$e_{xx}=e_{yy}=(S_{11}+S_{12})X\ ,\quad e_{zz}=2S_{12}X\ ,\quad e_{xy}=e_{yz}=e_{zx}=0\ , \tag{30}$$

and Eqs. (27)–(29) give, respectively,

$$\frac{dE_{\Gamma_6}}{dX}=2a_cS^+\ , \tag{31a}$$

$$\left[\frac{dE_{X_6}}{dX}\right]_z=2E_1S^+-\tfrac{2}{3}E_2S^-\ , \tag{31b}$$

$$\left[\frac{dE_{X_6}}{dX}\right]_{xy}=2E_1S^++\tfrac{1}{3}E_2S^-\ , \tag{31c}$$

$$\frac{dE_{L_6}}{dX}=2E_1'S^+\ , \tag{31d}$$

$$\frac{dE_{\rm hh}}{dX}=2a_vS^+-bS^-\ , \tag{31e}$$

$$\frac{dE_{\rm lh}}{dX}=2a_vS^++bS^-\ , \tag{31f}$$

$$\frac{dE_{\rm sh}}{dX}=2a_vS^+\ , \tag{31g}$$

where $S^+=S_{11}+2S_{12}$, $S^-=S_{11}-S_{12}$, and hh, lh, and sh are the heavy-, light-, and split-off hole states.

Under a [100] uniaxial in-plane stress the strain components are

$$e_{xx}=S_{11}X\ ,\quad e_{yy}=e_{zz}=S_{12}X\ ,\quad e_{xy}=e_{yz}=e_{zx}=0\ , \tag{32}$$

and, neglecting state mixings, the energy modulations are given by

$$\frac{dE_{\Gamma_6}}{dX}=a_cS^+\ , \tag{33a}$$

$$\left[\frac{dE_{X_6}}{dX}\right]_z=E_1S^++\tfrac{2}{3}E_2S^-\ , \tag{33b}$$

$$\left[\frac{dE_{X_6}}{dX}\right]_{xy}=E_1S^+-\tfrac{1}{3}E_2S^-\ , \tag{33c}$$

$$\frac{dE_{L_6}}{dX}=E_1'S^+\ , \tag{33d}$$

$$\frac{dE_{\rm hh}}{dX}=a_vS^+-\tfrac{1}{2}bS^-\ , \tag{33e}$$

$$\frac{dE_{\rm lh}}{dX}=a_vS^++\tfrac{1}{2}bS^-\ , \tag{33f}$$

$$\frac{dE_{\rm sh}}{dX}=a_vS^+\ . \tag{33g}$$

The piezomodulation amplitude of an electron-hole, or excitonic transition is then given by the difference between an equation like (31) or (33a)–(33d) and an equation like (31) or (33e)–(33g). At this point, two remarks are appropriate. First, concerning the hole-state modulation, it appears that the uniaxial configuration gives rise to the same type of modulation as the coplanar one, but with an amplitude 2 times smaller. As a result, this configuration is a most interesting one for hole-state identification. Second, if the heterostructure has a type-I configuration, electrons and holes are localized in the same material, so the hydrostatic deformation potentials that appear in the calculation are simply a_c-a_v, E_1-a_v, or $E_1'-a_v$, which are the band-gap deformation potentials. These parameters are generally known. If, instead, the heterostructure has a type-II configuration, electrons and holes are localized in different materials, so the differences that appear in the calculation are $a_{c_i}-a_{v_j}$, $E_{1_i}-av_j$, or $E'_{1_i}-a_{v_j}$. In this case, to carry out the calculation one needs to know, independently, the conduction- and valence-band deformation potentials of each material. This is not obvious, because the experimentally measured hydrostatic deformation potentials are almost exclusively the band-gap ones. Considering a_c and a_v, there exists several theoretical calculations—from the dielectric theory of the chemical bond,[15] from a self-consistent tight-binding treatment,[16] or from the linear muffin-tin-orbitals method[17]—which permit one to obtain the ratio a_c/a_v, and then to calculate a_c and a_v from the difference a_c-a_v. Concerning E_1 and E_1', Cardona *et al.* have given calculated values for several semiconductors.[17]

III. EXPERIMENTS

The sample piezomodulation is done by gluing the samples onto a piezoelectric transducer, such as lead zirconate titanate (PZT) ceramic, driven by an alternative voltage. Such transducers generate a change in length given by $\Delta l/l=dE$, where E is the electric field and d a piezoelectric parameter with a typical value of the order of 1 Å/V for PZT ceramics. The ac driving voltage is of the order of 100 V for a ceramic about 1 mm thick. This gives rise to an ac electric field of about 10^{-5} V/Å and then a strain $\Delta l/l$ of about 10^{-5}. Owing to the deformation-potential values of the zinc-blende-type semiconductors, the corresponding energy modulations are of the order of 0.1 meV. If the sample is glued only at its end, a uniaxial stress parallel to the sample surface is applied. If, instead, the whole sample surface is glued to a radial transducer, a coplanar stress is applied. When subjected to the alternating strain, the piezomodulated optical signals of the heterostructure display signatures characteristic of the electronic transition, and then of the electron and hole states involved. The piezomodulated signal is detected with standard lock-in technique, where the lock-in–detector reference is obtained from the ac stress driver.

A. Hole states

The optical techniques generally used to study the electron and holes states in heterostructures center on distin-

guishing different energy levels without additional information on the identity of the energy states. For instance, it is not obvious to experimentally identify the e-hh exciton states from the e-lh ones. PMS permits one to perform such an identification.

The ratio between the coplanar piezomodulation of the electron–light-hole and electron–heavy-hole transitions,

$$K_p=(dE_{e\text{-lh}}/dX)/(dE_{e\text{-hh}}/dX)\ ,$$

is given, from Eqs. (31), by

$$K_p=[2(a_c-a_v)S^+ + bS^-]/[2(a_c-a_v)S^+ - bS^-]\ . \quad (34)$$

A comparison between this piezomodulation and a nonselective modulation, such as the WMS, permits the identification of the transitions involved.

Let us first consider the most commonly studied heterostructure, GaAs/$Ga_{1-x}Al_xAs$. These structures have a type-I configuration, with electrons and holes localized within the GaAs layers. Using, for GaAs, the values $S_{11}=1.16\times10^{-6}$ bar^{-1}, $S_{12}=-0.37\times10^{-6}$ bar^{-1}, $a=a_c-a_v=-8.4$ eV, and $b=-1.76$ eV,[18] we obtain $K_p=2.2$. This shows that the electron–light-hole transitions are 2.2 times more piezomodulated than the electron–heavy-hole ones. In Fig. 2 we report the low-temperature differential-reflectivity spectra of GaAs/$Ga_{1-x}Al_xAs$ multiple-quantum-well structures, with aluminum content $x=0.25$, and well and barrier widths $L_z=60$ Å and $L_b=70$ Å, respectively. The pairs of structures that appear in the spectra result from interfacial defects of one atomic monolayer and have been studied elsewhere.[4] The piezomodulation spectrum corresponds to a coplanar configuration. The incident light is normal to a (001) face, with the stress applied in the [001] plane. In this experiment, the wavelength-modulated spectrum acts as a reference spectrum and allows one to compare the amplitude modulations of the piezomodulation spectrum. The ratio

$$(dE_{e_1\text{-lh}_1}/dX)/(dE_{e_1\text{-hh}_1}/dX)$$

of the amplitudes of the structures is K_w in WMS and K_p in PMS; clearly, $K_p\neq K_w$. In WMS, which is a nonselective modulation technique, the modulation parameter is the same for all the transitions, so that the ratio $K=K_p/K_w$ directly gives the ratio of the piezomodulation parameters of the (e_1-lh$_1$) and (e_1-hh$_1$) transitions. We find $K=2.6$. This is a value very close to the calculated one, which unambiguously identifies (e_1-lh$_1$) as an electron–light-hole transition and (e_1-hh$_1$) as an electron–heavy-hole transition. Figure 3 shows, for the same sample, the differential photoluminescence spectra, obtained in WMS and PMS. We measure the same value, $K=2.6$, for the ratio of the piezomodulation parameters of the two optical structures.

Let us now consider the case of CdTe epilayers on a

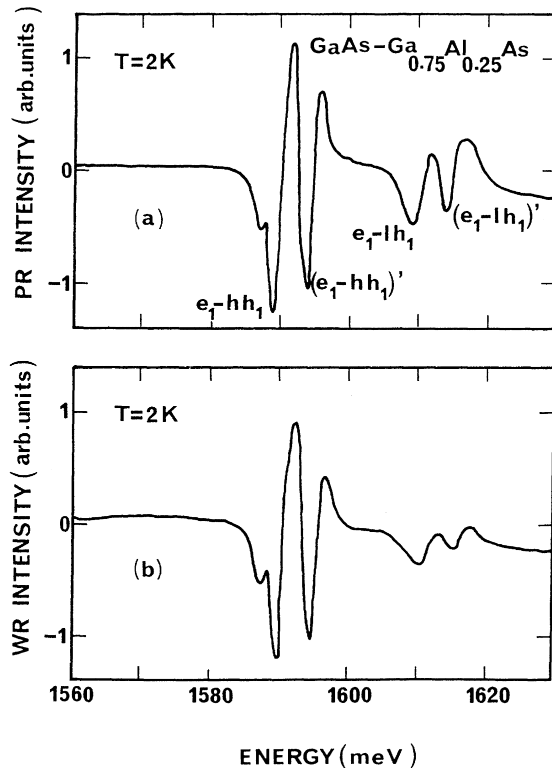

FIG. 2. Low-temperature differential-reflectivity spectra obtained on GaAs-$Ga_{1-x}Al_xAs$ multiple quantum wells by (a) piezomodulation and (b) wavelength-modulation techniques. In both spectra the first structure has been normalized to 1.

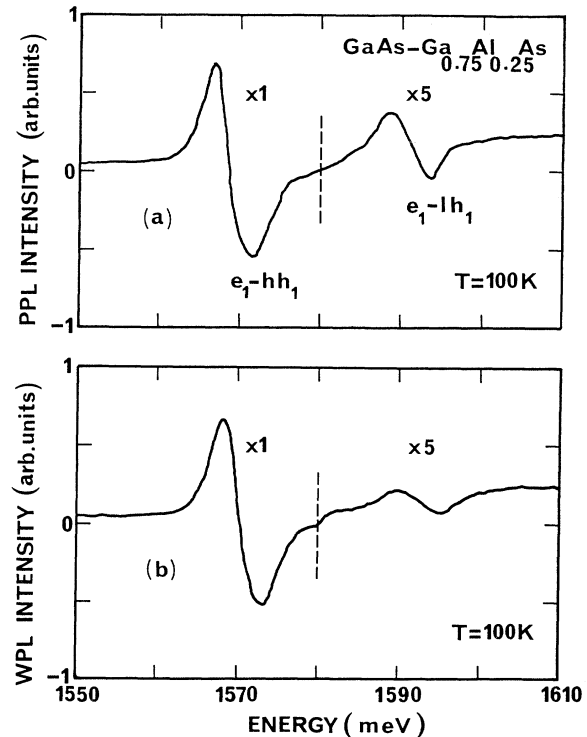

FIG. 3. 100-K differential-photoluminescence spectra. (a) Wavelength-modulation spectrum. (b) Piezomodulation spectrum.

[001] GaAs substrate. Owing to both the lattice mismatch between CdTe and GaAs and to the differential dilatation coefficient, the low-temperature CdTe epilayer experiences a biaxial stress giving rise to a splitting of the Γ_8 topmost valence band. Two structures corresponding to the valence-band–conduction-band transitions are expected, one associated with the electron–light-hole transition and the other with the electron–heavy-hole one. Using, for CdTe, the values $S_{11}=3.58\times10^{-6}$ bar^{-1}, $S_{12}=-1.39\times10^{-6}$ bar^{-1},[18] $a=a_c-a_v=-2.74$ eV,[19] and $b=-1.0$ eV,[3] we obtain, from Eq. (34), $K_p=-16$. We see that K_p is very large and negative. This means that not only are the electron–light-hole transitions much more modulated than the electron–heavy-hole ones, but, moreover, these transitions are modulated out of phase. The identification is then obvious. This is illustrated in Fig. 4, which shows the reflectivity spectrum of a molecular-beam-epitaxy–grown (MBE-grown) epilayer of CdTe on GaAs, together with the corresponding wavelength-modulated and coplanar piezomodulated spectra. Clearly, the transition labeled *e*-lh is much more modulated than that labeled *e*-hh. On the other hand, the higher-energy structures of spectra *b* and *c* are out of phase. This corresponds to the calculated value of K_p. Here, as in the previous case, the wavelength-modulated spectrum acts as a reference spectrum.

Another example concerning the identification of hole states is given by the strained-layer CdTe/ZnTe superlattices. It has been shown[20] that, depending on the layer thickness, these superlattices may have either a type-I configuration (where the electron and holes are mostly localized within the CdTe layers) or a type-II configuration

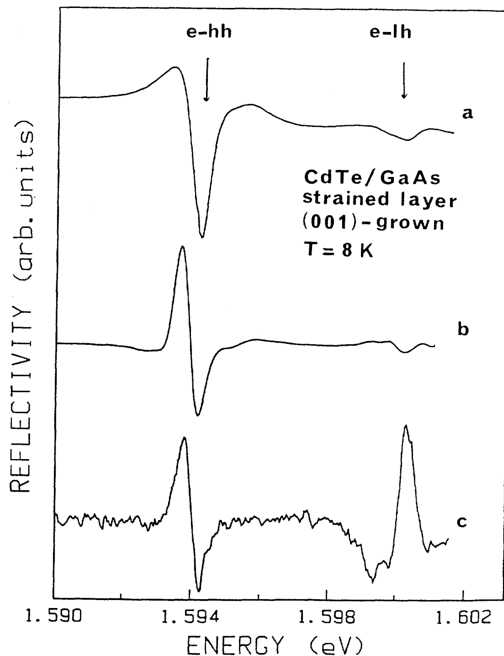

FIG. 4. Low-temperature reflectivity spectrum (labeled *a*) and differential-reflectivity spectra (labeled *b* and *c*) of a CdTe/GaAs epilayer. *b*, WMS; *c*, PMS.

(with the electron and heavy hole mostly localized within the CdTe layers and the light hole mostly localized within the ZnTe layers). Moreover, the hole ground state can be either a heavy-hole subband or a light-hole one. By using for CdTe the preceding values, with $a_c/a_v=1.9$,[15] and, for ZnTe, the values $S_{11}=2.38\times10^{-6}$ bar^{-1}, $S_{12}=-0.86\times10^{-6}$ bar^{-1},[21] $a_c-a_v=-5.3$ eV,[22] $a_c/a_v=1.9$,[15] and $b=-1.3$ eV,[21] we obtain from Eq. (31) for a coplanar modulation, $K_p=-16$ if both the heavy and light holes are localized within the CdTe layers, and $K_p=-13$ if the heavy holes are localized within the CdTe layers and the light holes within the ZnTe layers. In the study of these structures, piezomodulation spectroscopy is a powerful tool: First, it should give an unambiguous identification of the light- and heavy-hole states, because the transitions *e*-lh and *e*-hh are piezomodulated out of phase ($K<0$); secondly, it should precisely define the spatial localization of the holes, because $|K_p|$ is different depending on the light-hole localization.

As a last example, let us consider much more complicated structures such as at CdTe/$Cd_{1-y}Zn_yTe$ single quantum well, grown by MBE on a $Cd_{1-x}Zn_xTe$ [001] substrate. The epilayers are strained by the substrate, and the lattice mismatches induce a biaxial strain of both the $Cd_{1-y}Zn_yTe$ barrier and the CdTe well layer. Moreover, in the CdTe well the strain effect is combined with the confinement effect. As a result, a spectroscopic investigation exhibits a series of peaks involving both *e*-lh and *e*-hh transitions in either the CdTe well, the $Cd_{1-y}Zn_yTe$ barriers and the $Cd_{1-x}Zn_xTe$ substrate, or the buffer layer. On the other hand, when the electron-hole Coulombic interaction exceeds the sum of valence and conduction confinement energies, optical experiments[23,24] show the quantization of the exciton polariton instead of the confinement of electrons and holes separately. This is the case for CdTe when the well thickness is larger than about 200 Å. Consequently, identification of all the optical structures is far from obvious, and PMS appears once again to be a powerful tool in this case. Figure 5 shows different reflectivity and differential-reflectivity spectra concerning this type of heterostructure, with $x=0.03$, $y=0.08$, and a well thickness $L_w=450$ Å. As a result of the relation $0<x<y$, the lattice mismatches induce a biaxial dilatation of the $Cd_{1-y}Zn_yTe$ barriers and a biaxial compression of the CdTe well layer. First consider the optical structures labeled lh and hh on the reflectivity spectrum. A comparison between the wavelength-modulation (labeled *b*) and the coplanar piezomodulation (labeled *c*) spectra rather strikingly shows that the lh structure is much more piezomodulated than the hh one; moreover, these modulations are out of phase. This unambiguously identifies lh as an electron–light-hole transition and hh as an electron–heavy-hole one. Now, in addition to this identification, it clearly appears that hh is localized at a higher energy than lh; consequently, the layer involved is under biaxial dilatation. This identifies the spatial localization of the corresponding electronic transitions as being within the $Cd_{1-y}Zn_yTe$ barrier. Let us now consider the optical structures localized within the well, and labeled 1 and 2 in the reflectivity spectrum.

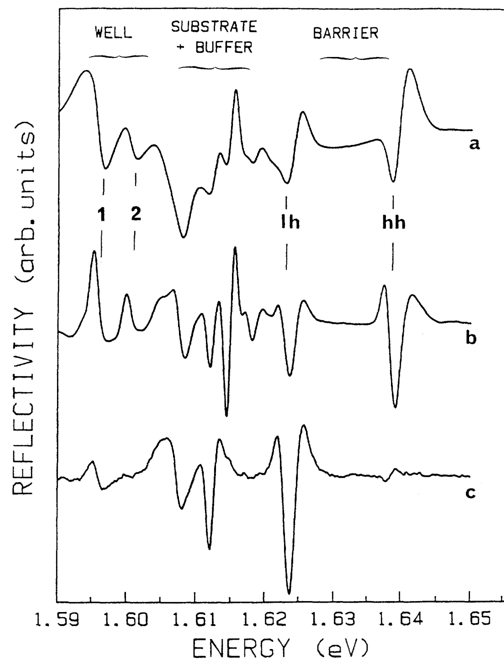

FIG. 5. Low-temperature reflectivity spectrum (labeled *a*) and differential-reflectivity spectra of CdTe-$Cd_{1-y}Zn_yTe$ single quantum well on a $Cd_{1-x}Zn_xTe$ substrate, with $x=0.03$, $y=0.08$, and well thickness $L_w=450$ Å. *b* is the wavelength-modulation spectrum and *c* the coplanar piezomodulation spectrum.

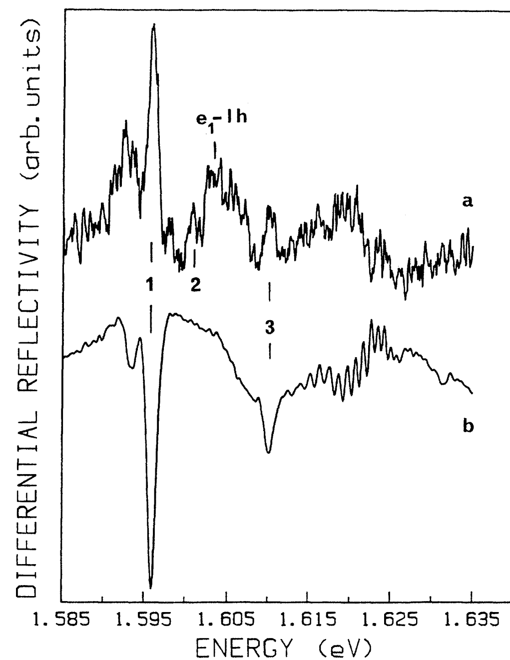

FIG. 6. Low-temperature differential-reflectivity spectra of CdTe/$Cd_{1-y}Zn_yTe$ single quantum well on a $Cd_{1-x}Zn_xTe$ substrate with $x=0.04$, $y=0.13$, and well thickness $L_w=180$ Å. *a*, coplanar piezomodulation spectrum; *b*, wavelength-modulation spectrum.

From the reflectivity spectrum alone, it is not obvious whether these transitions correspond to electron–light-hole or electron–heavy-hole transitions. A comparison between modulated spectra *b* and *c* answers the question. Since both structures 1 and 2 are weakly piezomodulated, both correspond to an electron–heavy-hole transition. Now, envelope-function calculations suggest that one identify these structures with the $N=1$ and 2 states of the electron–heavy-hole *e*-*h* confined exciton rather than the e_1-h_1 and e_2-h_2 transitions.[25] The ground light-hole state does not appear in these spectra. This results from the $Cd_{1-y}Zn_yTe$-layer light-hole localization. The electron–light-hole system has a type-II configuration and is weakly radiative in this sample. Type-II light-hole-related transitions were observed for quantum wells grown with higher zinc concentration in the barrier. Figure 6 shows differential-reflectivity spectra of a quantum well with $x=0.04$, $y=0.13$, and well thickness $L_w=180$ Å. In addition to the confined-exciton-related structures labeled 1, 2, and 3 and discussed above, the piezomodulation spectrum exhibits a structure labeled e_1-lh that does not appear in the wavelength-modulation spectrum. The amplitude of this structure, which appears strongly enhanced in the piezomodulation spectrum compared to the wavelength-modulation one, suggests a light-hole contribution. This agrees with envelope-function calculations that confirm the e_1-lh character of the transition, with the electron confined within the CdTe well and the light hole localized within the $Cd_{1-y}Zn_yTe$ barrier, where it is not confined.[25] Note the noise level that appears on the piezomodulation spectrum of Fig. 6—this results from the following: the structures labeled 1, 2, and 3, associated with electron–heavy-hole transitions, have a strong oscillator strength because they correspond to type-I transitions, but they are weakly piezomodulated. Conversely, the structure labeled e_1-lh, associated with electron–light-hole transitions, is strongly piezomodulated, but corresponds to type-II transitions and, as such, has a weak oscillator strength.

B. Electron states

"Well" and "barrier" materials used in III-V and II-VI semiconductor heterostructures generally are direct-band-gap materials, so that electron states result from the Γ_6-electron confinement. The result is a series of electronic subbands clearly identified without any ambiguity. In contrast to these classical systems, GaAs/AlAs superlattices are quite peculiar because AlAs is an indirect-band-gap semiconductor whose lowest minimum of the conduction band is of X_6 symmetry. The relative ordering of the Γ_6 and X_6 extrema in each material, together with the valence-band offset, act in such a way that, depending on the relative thickness of GaAs and AlAs layers, both type-I and -II superlattices can be grown. For large-period superlattices, both electrons and holes are mostly localized within the GaAs layers, and the electron wave functions have Γ character. On the other hand, in short-period superlattices, on account of the low value of the Γ-electron effective mass, GaAs remains a well for the holes, but becomes a barrier for the electrons, and su-

perlattice has a type-II configuration.[26] In this case the electrons are mostly localized within the AlAs layers and their wave function is comprised of bulk states of X_6 symmetry. Moreover, on account of the mass anisotropy of the X minima, quantum confinement gives rise to an X_z subband and $X_{x,y}$ doubly-degenerate subbands. Because of the higher value of the longitudinal effective mass, the first X_z subband should be the ground state. However, in some structures the ordering between X_z and X_{xy} appears to be reversed by in-plane stress resulting from lattice mismatch between GaAs and AlAs.[27] In these superlattices the problem is then to identify the electron states between Γ, X_z, and X_{xy} states. PMS again answers the question. The ratios of the piezomodulation of the different electron–heavy-hole transitions,

$$A=(dE_{eX_z\text{-hh}}/dX)/(dE_{e\Gamma\text{-hh}}/dX) ,$$

$$B=(dE_{eX_{xy}\text{-hh}}/dX)/(dE_{e\Gamma\text{-hh}}/dX) ,$$

and

$$C=(dE_{eX_{xy}\text{-hh}}/dX)/(dE_{eX_z\text{-hh}}/dX) ,$$

for the coplanar configuration (A_p,B_p,C_p) and the uniaxial configuration (A_a,B_a,C_a) are given, from Eqs. (31) and (33) by

$$A_p=[(2E_1S^+-\tfrac{2}{3}E_2S^-)_{\text{AlAs}}-(2a_vS^++bS^-)_{\text{GaAs}}]/[2(a_c-a_v)S^+-bS^-]_{\text{GaAs}} , \tag{35a}$$

$$B_p=[(2E_1S^++\tfrac{1}{3}E_2S^-)_{\text{AlAs}}-(2a_vS^++bS^-)_{\text{GaAs}}]/[2(a_c-a_v)S^+-bS^-]_{\text{GaAs}} , \tag{35b}$$

$$C_p=[(2E_1S^++\tfrac{1}{3}E_2S^-)_{\text{AlAs}}-(2a_vS^++bS^-)_{\text{GaAs}}]/[(2E_1S^+-\tfrac{2}{3}E_2S^-)_{\text{AlAs}}-(2a_vS^++bS^-)_{\text{GaAs}}] , \tag{35c}$$

and

$$A_a=[(E_1S^++\tfrac{2}{3}E_2S^-)_{\text{AlAs}}-(a_vS^++\tfrac{1}{2}bS^-)_{\text{GaAs}}]/[(a_c-a_v)S^+-\tfrac{1}{2}bS^-]_{\text{GaAs}} , \tag{36a}$$

$$B_a=[(E_1S^+-\tfrac{1}{3}E_2S^-)_{\text{AlAs}}-(a_vS^++\tfrac{1}{2}bS^-)_{\text{GaAs}}]/[(a_c-a_v)S^+-\tfrac{1}{2}bS^-]_{\text{GaAs}} , \tag{36b}$$

$$C_a=[(E_1S^+-\tfrac{1}{3}E_2S^-)_{\text{AlAs}}-(a_vS^++\tfrac{1}{2}bS^-)_{\text{GaAs}}]/[(E_1S^++\tfrac{2}{3}E_2S^-)_{\text{AlAs}}(a_vS^++\tfrac{1}{2}bS^-)_{\text{GaAs}}] . \tag{36c}$$

By using, for AlAs, the compliance constants of GaAs given above, and for the deformation potentials the measured values $E_1-a_v=1.4$ eV (Ref. 28) and $E_2=5.1$ eV (Ref. 29), we get

$$A_p=0.30,\quad B_p=-1.5,\quad C_p=-4.5$$

and

$$A_a=-3.3,\quad B_a=0.30,\quad C_a=-0.09 .$$

Clearly, the X_z and X_{xy} subbands appear to be piezomodulated out of phase ($C_{a,p}<0$). Moreover, in the coplanar configuration, the eX_z-hh transition is less modulated than the $e\Gamma$-hh transition, but the eX_{xy}-hh transition is more modulated. On the other hand, C_a, which is small and negative, shows that in the uniaxial configuration the eX_z-hh transition is about 30 times more modulated than the eX_{xy}-hh transition. Identification of the electron states is then possible.

As an illustration, Fig. 7 shows the low-temperature luminescence and differential-luminescence spectra of a short-period GaAs/AlAs superlattice. The superlattice has a period of 30.1 Å with a relative thickness of AlAs of $\bar{x}\simeq 60\%$, and is composed of 2×357 periods separated by an enlarged well of GaAs of 32 Å. The luminescence spectrum, labeled a, exhibits two structures, one associated with the superlattice and the other with the isolated GaAs quantum well. On account of both the well width and the GaAs-layer thickness of the superlattice, the

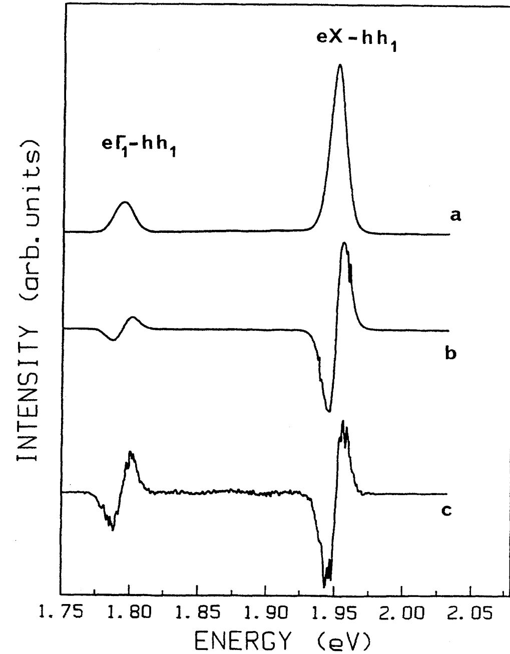

FIG. 7. Low-temperature photoluminescence spectra of GaAs/AlAs short-period superlattice containing an enlarged GaAs quantum well. a, direct photoluminescence spectrum; b, wavelength-modulation spectrum; c, piezomodulation spectrum.

low-energy structure corresponds to $e\Gamma_1$-hh_1 transitions localized inside the isolated well, and the high-energy one corresponds to eX-hh_1 transitions of the superlattice, which has a type-II configuration. Now the question is: Is the superlattice electron state X_z- or X_{xy}-like? A comparative study of the wavelength-modulated (labeled b) and piezomodulated (labeled c) differential spectra of Fig. 7 answers this question. First, it clearly appears that spectra b and c have the same shape, so that the eX-hh_1 and $e\Gamma_1$-hh_1 transitions are piezomodulated in phase. Now, the calculated values of

$$A_p = (dE_{eX_z\text{-hh}}/dX)/(dE_{e\Gamma\text{-hh}}/dX)$$

and

$$B_p = (dE_{eX_{xy}\text{-hh}}/dX)/(dE_{e\Gamma\text{-hh}}/dX)$$

are, respectively, positive $(+0.30)$ and negative (-1.5). This unambiguously identifies the experimental eX-hh_1 structure as a (eX_z-hh)-like transition. Moreover, the measured piezomodulation ratio

$$(dE_{eX\text{-hh}_1}/dX)/(dE_{e\Gamma\text{-hh}_1}/dX)$$

is 0.33, which is very close to the calculated value of $A_p = 0.30$. This clearly identifies the electron ground state of this superlattice as an X_z-like state.

IV. CONCLUSIONS

In conclusion, we have shown that a comparative study of piezomodulated and wavelength-modulated spectroscopies is a sensitive experimental tool which allows one to identify electron and/or hole states, together with spatial localizations in strained epilayers, quantum wells, and superlattices. Several aspects of the present study merit further investigation, and a more accurate quantitative study of the piezomodulation amplitude should give information on the confined-state deformation potentials. A comparison with the bulk deformation potentials would then give the components of the confined-state wave functions.

ACKNOWLEDGMENTS

We are grateful to A. Regreny for providing GaAs/$Ga_{1-x}Al_xAs$ quantum wells, to J. P. Faurie for providing CdTe/ZnTe superlattices, to J. Cibert for providing CdTe/GaAs epilayers, to H. Mariette for providing CdTe/$Cd_{1-y}Zn_yTe$ quantum wells, and to R. Planel for providing GaAs/AlAs short-period superlattices.

[1]B. O. Seraphin, in *Optical Properties of Solids*, edited by F. Abelès (North-Holland, Amsterdam, 1972), p. 163; *Modulation Techniques*, Vol. 9 of *Semiconductors and Semimetals*, edited by R. K. Willardson and A. C. Beer (Academic, New York, 1972); W. E. Engeler, H. Fritzche, M. Garfinkel, and J. J. Tiemann, Phys. Rev. Lett. **14**, 1069 (1965); D. D. Sell, Surf. Sci. **37**, 896 (1973).

[2]Y. R. Lee, A. K. Ramdas, L. A. Kolodzoejsko, and R. L. Gunshor, Phys. Rev. B **38**, 13 143 (1988).

[3]J. Allègre, B. Gil, J. Calatayud, and H. Mathieu, in Proceedings of the 4th International Conference on II-VI Compounds, Berlin, 1989 [J. Cryst. Growth **101**, 603 (1990)].

[4]H. Mathieu, P. Lefebvre, J. Allègre, B. Gil, and A. Regreny, Phys. Rev. B **36**, 6581 (1987).

[5]F. Dal'bo, N. Magnea, G. Lentz, H. Mariette, B. Gil, J. Allègre, and H. Mathieu, in *Proceedings of the 19th International Conference on the Physics of Semiconductors*, Varsovie, 1988, edited by W. Zawadzki (Institute of Physics/Polish Academy of Sciences, Warsaw, 1988), p. 643.

[6]A. K. Ramdas, Superlatt. Microstruct. **4**, 69 (1988).

[7]Y. R. Lee, A. K. Ramdas, F. A. Chambers, J. M. Meese, and L. R. Ram-Mohan, Appl. Phys. Lett. **50**, 600 (1987).

[8]Y. R. Lee, A. K. Ramdas, F. A. Chambers, J. M. Meese, and L. R. Ram-Mohan, Mod. Opt. Charact. Technol. Semicond. Devices **794**, 105 (1987).

[9]G. Lasher and F. Stern, Phys. Rev. **133**, A553 (1964).

[10]B. O. Seraphin and N. Bottka, Phys. Rev. **145**, 628 (1966).

[11]D. E. Aspnes and A. A. Studna, Phys. Rev. B **27**, 985 (1983).

[12]H. Brooks, in *Advances in Electronics and Electron Physics*, edited by L. Marton (Academic, New York, 1955), Vol. 5, p. 85.

[13]M. Chandrasekhar and F. H. Pollak, Phys. Rev. B **15**, 2121 (1977).

[14]H. Mathieu, P. Merle, E. L. Ameziane, B. Archilla, and J. Camassel, Phys. Rev. B **19**, 2209 (1979).

[15]D. L. Camphausen, G. A. N. Connel, and W. Paul, Phys. Rev. Lett. **26**, 184 (1971).

[16]C. Priester, G. Allan, and M. Lannoo, Phys. Rev. B **38**, 13 451 (1988), and private communication.

[17]M. Cardona and N. E. Christensen, Phys. Rev. B **35**, 6182 (1987).

[18]D. J. Olego, J. Petruzzello, S. K. Ghandi, N. R. Taskar, and I. B. Bhat, Appl. Phys. Lett. **51**, 127 (1987).

[19]D. J. Dunstan, B. Gil, C. Priester, and K. P. Homewood, Semicond. Sci. Technol. **4**, 241 (1989).

[20]H. Mathieu, J. Allègre, A. Chatt, P. Lefebvre, and J. P. Faurie, Phys. Rev. B **38**, 7740 (1988).

[21]W. Wardzynski, W. Giriat, H. Szymezak, and R. Howalczyk, Phys. Status Solidi B **49**, 71 (1972).

[22]K. Strossmer, S. Ves, C. K. Kim, and M. Cardona, Solid State Commun. **61**, 275 (1987).

[23]H. Tuffigo, R. T. Cox, Y. Merle d'Aubigné, and A. Million, Phys. Rev. B **37**, 4310 (1987).

[24]H. Tuffigo, R. T. Cox, G. Lentz, N. Magnea, and H. Mariette, in Proceedings of the 4th International Conference on II-VI Compounds, Berlin, 1989 [J. Cryst. Growth **101**, 778 (1990)].

[25]J. Allègre, J. Calatayud, B. Gil, H. Mathieu, H. Tuffigo, G. Leutz, N. Magnea, and H. Mariette, Phys. Rev. B **41**, 8195 (1990).

[26]G. Danan, B. Etienne, F. Mollot, R. Planel, A. M. Jean Louis, F. Alexandre, B. Jusserand, G. Leroux, J. Y. Marzin, H. Savary, and B. Sermage, in *Proceedings of the 18th International Conference on the Physics of Semiconductors*, Stockholm, 1986, edited by O. Engström (World Scientific, Singapore, 1986), p. 719; Phys. Rev. B **35**, 6027 (1987).

[27]P. Lefebvre, B. Gil, H. Mathieu, and R. Planel, Phys. Rev. B **39**, 5550 (1989).

[28]F. Minami, K. Todori, and K. Inoue, Semicond. Sci. Technol. **4**, 265 (1989).

[29]P. Lefebvre, B. Gil, H. Mathieu, and R. Planel, Phys. Rev. B **40**, 7802 (1989).